Efficient Third-Harmonic Generation From 2 μm in Asymmetric Plasmonic Slot Waveguide

Tianye Huang, Member, IEEE
Xuguang Shao
Zhifang Wu
Timothy Lee
Tingting Wu
Yunxu Sun
Jing Zhang
Huy Quoc Lam
Gilberto Brambilla
Perry Ping Shum, Senior Member, IEEE
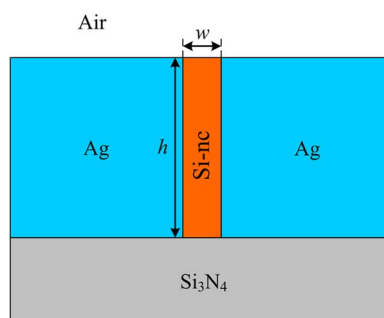
Efficient Third-Harmonic Generation From 2 μm in Asymmetric Plasmonic Slot Waveguide

Tianye Huang,[1,2] *Member, IEEE*, Xuguang Shao,[1,2] Zhifang Wu,[1,2] Timothy Lee,[3] Tingting Wu,[2,6] Yunxu Sun,[2,6] Jing Zhang,[4] Huy Quoc Lam,[5] Gilberto Brambilla,[3] and Perry Ping Shum,[1,2] *Senior Member, IEEE*

[1]CINTRA CNRS/NTU/THALES, UMI 3288, Singapore 639798
[2]School of Electrical and Electronics Engineering, Nanyang Technological University, Singapore 639798
[3]Optoelectronics Research Center, University of Southampton, Southampton, SO17 1BJ, U.K.
[4]National Metrology Centre, Agency for Science, Technology, and Research (A∗STAR), Singapore 118221
[5]Temasek Laboratories, Nanyang Technological University, Singapore 117411
[6]Shenzhen Graduate School, Harbin Institute of Technology, Shenzhen 150090, China

Abstract: We propose the asymmetrical plasmonic slot waveguide (APSW) design for third-harmonic generation (THG) from 2.25 μm. In this configuration, the phase-matching condition is fulfilled between the zeroth-order mode at fundamental frequency (FF) and the first-order mode at third-harmonic frequency (THF). Due to the asymmetrical geometry, the mode overlap between the two involved modes is significantly enhanced, leading to an efficient THG process. According to the numerical calculation, the conversion efficiency is predicted up to 1.4% with 1-W pump power. The proposed APSW has the potential to realize an integrated efficient THG device in nanometer scale.

Index Terms: Nonlinear optical signal processing, harmonic generation and mixing, fiber optics and optical communications.

1. Introduction

In order to fulfill the requirement of high data rate and high capacity for future telecommunication link, the 2-μm band is stimulating interest in fiber optical communication system where there is the prospect of developing low-loss, low-latency transmission systems based on hollow core band gap fibers [1], [2]. Meanwhile, the development of Thulium-doped fiber lasers accelerates the research of nonlinear photonics in this special waveband and makes nonlinear optics possible [3]. Accompany with the development of this special waveband, various all-optical integrated functional devices for signal processing such as dispersion/OSNR monitoring, switching, wavelength conversion and so on are highly desired. Third harmonic generation (THG) has been demonstrated as a promising candidate to realize high speed optical performance monitoring of in-band OSNR and residual dispersion in C-band [4], therefore pursuing efficient THG devices working in longer
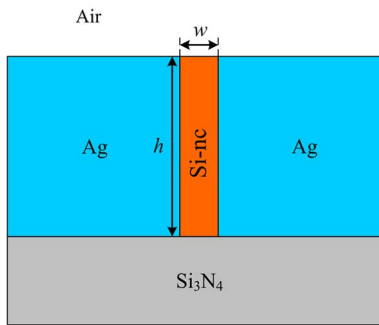
Fig. 1. Cross-section view of the proposed APSW.

wavelength is reasonable and valuable. Furthermore, THG can also find applications on microscopy [5], scanning microscopy [6], and light emission [7].

Typically, efficient THG process depends on three key points, namely nonlinearity of interactive material, overlap integral between fundamental and harmonic modes, and phase-matching conditions. However, these above-mentioned characteristics are quite difficult to be fulfilled, simultaneously. For example, in silica microfibers [8], good modal overlap and phase matching can be achieved between HE_{11} mode at pump wavelength and HE_{12} at harmonic wavelength. However, because of the small nonlinear optical susceptibility $\chi^{(3)}$ in silica glasses, efficient THG is difficult to be realized in short microfibers. Phase-matched THG has been demonstrated in highly germanium-doped fiber [9], but the conversion efficiency suffers from the small overlap integral between mode HE_{11} and HE_{13}. Comparing with silica, tellurite and chalcogenide glasses with much higher $\chi^{(3)}$ can be more promising platforms for THG. The challenges lie in proper fiber design is required to realize good mode overlap and phase-matching [10], [11]. THG was also investigated in slow light silicon-based photonic crystal waveguide [4], [12]. In this configuration, the nonlinearity of the interactive medium is significantly enhanced by the slow light effect but the fundamental mode can only phase match the leaky modes or radiation modes at harmonic wavelengths.

Among those approaches, waveguide-based THG configurations with large nonlinearity have the potential to further reduce the footprints and power consumption of the devices. However, in order to hit the target, advanced device design is required to fulfill the three above-mentioned key points, namely high nonlinear interactive medium, large mode overlap, and proper phase-matching condition. Recently, plasmonic waveguides are of great interests because of their ability to allow strong local-enhance confinement of light beyond the limits of diffraction in dielectric media [13], [14]. Additionally, by tailoring the mode dispersion in these waveguides, phase-matching between two modes with large overlap is also possible [15]. Based on these features, it is no surprise that plasmonic waveguides are of great potential to realize highly efficient THG devices. In this paper, we propose an asymmetric plasmonic slot waveguide (APSW) configuration with highly nonlinear silicon nanocrystal (Si-nc) as its interactive medium embedding in the slot region. This configuration is able to tightly confine both fundamental frequency (FF) and third-harmonic frequency (THF) in the highly nonlinear slot region and significantly break the symmetry of first-order mode at THF leading to large mode overlap. Furthermore, by carefully optimizing the waveguide geometry, phase-matching condition can also be satisfied. With fundamental pump wavelength at 2.25 μm, the performance of the proposed APSW was analyzed by numerical simulations.

2. Waveguide Design

The cross-section geometry of the proposed APSW is demonstrated in Fig. 1. The metallic slot with height h and width w formed by sliver is filled with silicon nanocrystal (Si-nc) with high nonlinear refractive index of 4.8×10^{-17} m^2/w [16]. The material dispersion of Si-nc with silicon excess of 8% is given in [17] while the Drude permittivity dispersion of sliver is given by $\varepsilon_{Ag} = \varepsilon_\infty - f_p^2/[(f(f + i\gamma)],$
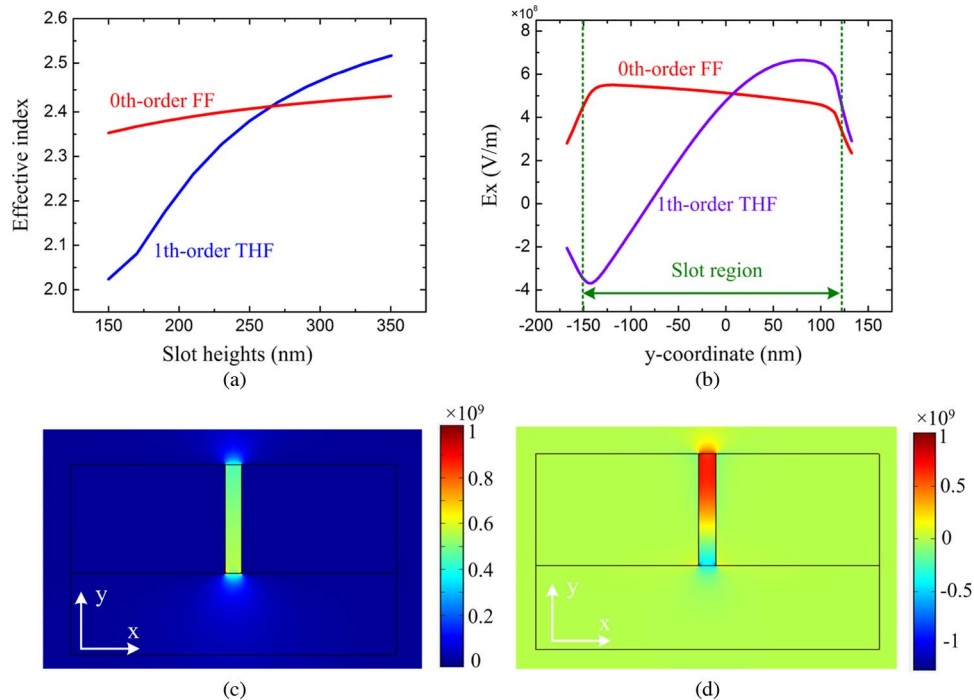
Fig. 2. (a) Effective indices of the 0th-order mode at FF and 1st-order mode at THF versus the slot height h when the slot width is fixed to be 40 nm; (b) E_x distribution at x = 0 of the 0th-order mode at FF and 1st-order mode at THF; (c) E_x profile of 0th-order mode at FF; (d) E_x profile of 1st-order mode at THF. (b–d) are plotted at phase-matching condition w = 40 nm, h = 265.1 nm.

with $\varepsilon_\infty = 5$, $f_p = 2175$ THz, and $\gamma = 4.35$ THz [18]. The substrate is formed by Si_3N_4, and the whole device is surrounded by air.

In the process of THG in optical waveguide supporting several modes, three pump photons, oscillating at the circular frequency ω_1 with propagation constant β_1, combines into a single photon with circular frequencies $\omega_3 = 3\omega_1$ and the propagation constant difference $\Delta\beta = \beta_3 - 3\beta_1 \approx 0$. This condition is equivalent to: $n_{eff}(\omega_1) \approx n_{eff}(\omega_3)$, where n_{eff} is the effective index of the relevant mode. In this paper, we consider the phase-matching condition between 2.25 μm and 0.75 μm. The main approaches to realize phase-matching in optical fibers or waveguides including quasi-phase-matching technique [19] and inter-modal phase-matching technique [8], [9]. To realize quasi-phase-matching, index grating should be inscribed in the optical fiber. However, the fabrication process can be quite complicated. While inter-modal phase-matching technique makes use of the distinction of the modal dispersion properties between FF and THF which can be achieved by properly designing the waveguide geometry. In general, in a waveguide that supports several modes, the effective index of the fundamental mode is larger than the high-order mode at a specified frequency. On the other hand, for most material, the refractive indices increase with frequency. Therefore, phase-matching can be fulfilled if the FF propagates in a lower-order mode while the THF propagates in a higher-order mode. This technique is more flexible because no post-processing is required after waveguide fabrication. In our proposed configuration, inter-modal phase-matching technique is adopted.

Firstly, the slot width w is fixed to be 40 nm. Fig. 2(a) shows effective indices of the 0th-order mode at FF ($\lambda_1 = 2.25$ μm) and 1st-order mode at THF ($\lambda_3 = 0.75$ μm) versus the slot height h. It can be easily found that there is a cross point between the two modes when $h = 265.1$ nm, indicating specified waveguide geometry for phase-matching. Using a full-vector finite element method (FEM) simulator (COMSOL. Multiphysics), the effective indices at FF and THF are calculated to be $2.412667 + 0.011205i$ and $2.412662 + 0.009316i$. Because Si-nc possesses very low extinction
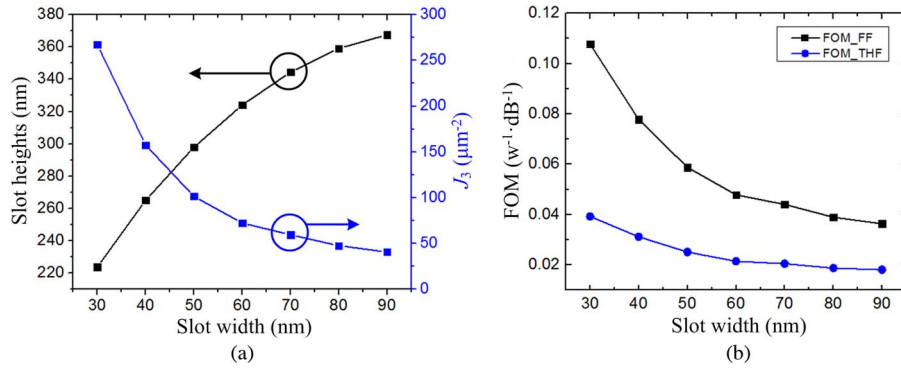
Fig. 3. (a) Slot height and width pairs that satisfy phase-matching condition and corresponding J_3; (b) FOM of FF and THF versus slot width at phase-matching condition.

coefficient (less than 10^{-4}) near THF comparing to sliver [20], the loss of Si-nc is neglected in the simulation. The x-polarized electrical field E_x are demonstrated in Fig. 2(b)–(d). Obviously, for 0th-order mode at FF, the electrical components are all positive, while the 1st-order mode at THF preserves both positive and negative parts which contribute oppositely to overlap integration with FF mode for THG. However, because of the substrate and top of the proposed APSW is composed by different material, namely, Si_3N_4 and Air, the symmetry of the 1st-order mode is significantly broken resulting small counteraction effect when calculating overlap integral with FF mode.

It should be noted that the specified w and h mentioned above is not the only case for phase-matching. In Fig. 3(a), with different w, slot height h is optimized to satisfy phase-matching condition. In THG process, one of the key parameters is the overlap integral J_3 that directly relates to the power transfer between FF and THF. This parameter is calculated according to [21]

$$J_3 = \iint\limits_{A_{NL}} \left(F_1^* \cdot F_3 \right) \left(F_1^* \cdot F_1^* \right) dS. \tag{1}$$

In Fig. 3(a), it can be found that J_3 goes down with increased slot width due to the stronger confinement of the field with smaller area. However, in the proposed APSW, besides J_3, propagation attenuation is another aspect which must be paid attention to, since a portion of the field is in contact with metal area leading to high loss to the FF and THF mode. In order to evaluate the features of the APSW at different phase-matching conditions, we define the figure-of-merit (FOM) for phase-matched THG process as

$$FOM_{FF,THF} = \frac{n^{(2)} k_{FF} J_3}{\alpha_{FF,THF}} \tag{2}$$

where $n^{(2)}$ denotes to the nonlinear refractive index of the interactive medium, $k_{FF} = 2\pi/\lambda_{FF}$, and α_{FF} and α_{THF} are the propagation loss at FF and THF, respectively. At difference phase-matching conditions, the FOMs are illustrated in Fig. 3(b). It can be found that both FOM_{FF} and FOM_{THF} go down with slot width increment, which means the APSW has better THG performance with smaller width. However, for practical application, the fabrication feasibilities must be taken into consideration and slot width cannot be too narrow.

To further emphasize the contribution of the asymmetrical geometry, we also consider the configuration with Si_3N_4 covering the top of the waveguide with slot width of 40 nm. In this case, phase-matching condition is fulfilled when $h = 159.4$ nm. However, J_3 is quite small with a value of only 0.16 μm^{-2} and the corresponding FOM_{FF} and FOM_{THF} are 7.7×10^{-5} $w^{-1} \cdot dB^{-1}$ and 1.8×10^{-5} $w^{-1} \cdot dB^{-1}$, respectively, which is $\sim$1000 times or $\sim$1600 times smaller compared with the values in APSW.
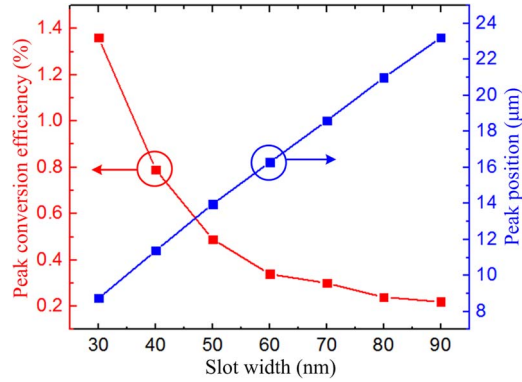
Fig. 4. Peak conversion efficiencies of THG with 1 w pump and their corresponding positions at different phase-matching conditions.
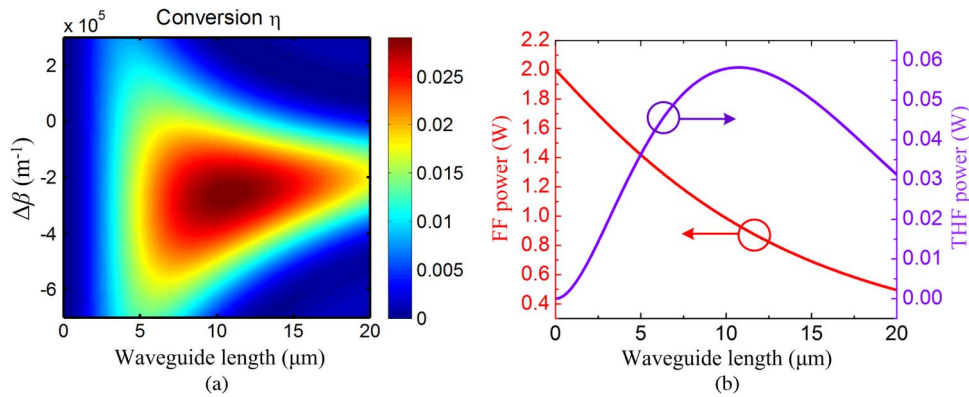

Fig. 5. (a) Contour map of conversion efficiency with 2 w pump power, and (b) FF and THF power evolution when $\Delta\beta = -2.6 \times 10^5$ m^{-1}.

3. THG in the Proposed APSW

Assuming the fields at FF and THF are in different but single propagating modes of the fiber, the fields can be described by slowly varying amplitudes $A_i(z)$, where $i = 1$ refers to the FF, and $i = 3$ refers to the THF. The following set of equations can then be derived [21]:

$$\frac{\partial A_1}{\partial z} = -\frac{\alpha_1}{2} A_1 + i\gamma_0 \left[\left(J_1 |A_1|^2 + 2J_2 |A_3|^2 \right) A_1 + J_3 \left(A_1^* \right)^2 A_3 e^{i\Delta\beta z} \right] \tag{3}$$

$$\frac{\partial A_3}{\partial z} = -\frac{\alpha_3}{2} A_3 + i\gamma_0 \left[\left(6J_2 |A_1|^2 + 3J_5 |A_3|^2 \right) A_3 + J_3^* A_1^3 e^{-i\Delta\beta z} \right] \tag{4}$$

where J_1, J_2, J_3, and J_5 denote the modal overlap integrals for FF modulation (SPM), FF-THF cross-phase modulation (XPM), FF-THF conversion, and FF SPM, α_i is the loss coefficient, $\Delta\beta$ is the propagation constant mismatch, and $\gamma_0 = 2\pi n^{(2)}/\lambda_{\text{FF}}$, where $n^{(2)}$ is the nonlinear refractive index coefficient. For a lossy interaction, the THG conversion efficiency is given by $\eta = P_{3\text{out}}/P_1(0)$, where $P_{3\text{out}}$ is the power of the THF at the output and $P_1(0)$ is the input FF power. Assuming a pump power of 1 W, the peak conversion efficiency and corresponding waveguide length are demonstrated in Fig. 4. It can be seen that the achievable η_{max} increases with narrower slot width together with shorter required waveguide length. These results are consistent with the FOM variation at different phase-matching conditions. Although the maximum peak efficiency demonstrated here is ~1.4%, it should be noted that this value can be further increased by higher pump power. In Fig. 5(a), with 2 W pump power, a contour map of conversion efficiency with respected to $\Delta\beta$ and waveguide length is plotted

when slot width is 40 nm. Obviously, with higher pump power, the conversion efficiency is improved while interaction length is also reduced. At this pump level, the peak conversion efficiency is higher than 2.9%. The required waveguide length to achieve maximum THF power is 10.7 μm, as shown in Fig. 5(b). Therefore, the proposed APSW has the potential for future integrated photonic circuit with μm-scale. It should be noted that Si-nc demonstrates two photon absorption (TPA) at THF. This nonlinear process can act as additional loss mechanism and limit the output power of THF at high pumping level. However, TPA is strongly dependent on the power intensity of the generated THF while the linear absorption induced by metal is already quite large. According to the nonlinear absorption coefficient $\sim 10^{-9}$ m/W of Si-nc reported in [20], [22], it can be estimated that if the power of generated THF is lower than 100 mw, the impact of TPA is negligible and the total loss is still dominated by linear absorption.

4. Conclusion

In summary, we have designed APSW for phase-matched THG and analyzed the performances for different phase-matching conditions which are satisfied between 0th-order mode at FF and 1st-order mode at THF. Because of the substrate and top of the proposed APSW is composed by different material, namely, Si_3N_4 and Air, the symmetry of the 1st-order mode is significantly broken resulting large overlap with the 0th-order mode. According to our calculation, $\sim$1.4% THG efficiency is predicted with 1 W pump. While higher efficiency up to 2.9% is also achievable in μm-scale waveguide with enhanced pump power level. The proposed APSW has the potential to realize high efficiency integrated THG devices.

References

[1] F. Poletti *et al.,* "Towards high-capacity fibre-optic communications at the speed of light in vacuum," *Nat. Photon.,* vol. 7, no. 4, pp. 279–284, Apr. 2013.

[2] Z. Li, S. U. Alam, Y. Jung, A. M. Heidt, and D. J. Richardson, "All-fiber, ultra-wideband tunable laser at 2 μm," *Opt. Lett.,* vol. 38, no. 22, pp. 4739–4742, Nov. 2013.

[3] I. Kubat *et al.,* "Thulium pumped mid-infrared 0.9-9 μm supercontinuum generation in concatenated fluoride and chalcogenide glass fibers," *Opt. Exp.,* vol. 22, no. 4, pp. 3959–3967, Feb. 2014.

[4] B. Corcoran *et al.,* "Optical signal processing on a silicon chip at 640 Gb/s using slow-light," *Opt. Exp.,* vol. 18, no. 8, pp. 7770–7781, Apr. 2010.

[5] I. Appelbaum, "Tunnel conductance spectroscopy via harmonic generation in a hybrid capacitor device," *Appl. Phys. Lett.,* vol. 103, no. , pp. 122 604-1–122 604-4, Sep. 2013.

[6] D. Sandkuij, A. E. Tuer, D. Tokarz, J. E. Sipe, and V. Barzda, "Numerical second- and third-harmonic generation microscopy," *J. Opt. Soc. Amer. B, Opt. Phys.,* vol. 30, no. 2, pp. 382–395, Feb. 2013.

[7] B. Corcoran *et al.,* "Green light emission in silicon through slow-light enhanced third-harmonic generation in photonic-crystal waveguides," *Nat. Photon.,* vol. 3, no. 4, pp. 206–210, Apr. 2009.

[8] T. Lee *et al.,* "Broadband third harmonic generation in tapered silica fibres," *Opt. Exp.,* vol. 20, no. 8, pp. 8503–8511, Apr. 2012.

[9] K. Bencheikh *et al.,* "Phase-matched third harmonic generation in highly germanium-doped fiber," *Opt. Lett.,* vol. 37, no. 3, pp. 289–291, Feb. 2012.

[10] A. Lin, A. Ryasnyanskiy, and J. Toulouse, "Tunable third-harmonic generation in a solid-core tellurite glass fiber," *Opt. Lett.,* vol. 36, no. 17, pp. 3437–3439, Sep. 2011.

[11] T. Chen *et al.,* "Tunable third-harmonic generation in a chalcogenide-tellurite hybrid optical fiber with high refractive index difference," *Opt. Lett.,* vol. 39, no. 4, pp. 1005–1007, Feb. 2014.

[12] C. Monat *et al.,* "Investigation of phase matching for third-harmonic generation in silicon slow light photonic crystal waveguides using Fourier optics," *Opt. Exp.,* vol. 18, no. 7, pp. 6831–6840, Mar. 2010.

[13] M. Kauranen and A. V. Zayats, "Nonlinear plasmonics," *Nat. Photon.,* vol. 6, no. 11, pp. 737–748, Nov. 2012.

[14] M. I. Stockman, "Nanoplasmonics: Past, present, and glimpse into future," *Opt. Exp.,* vol. 19, no. 22, pp. 22 029–22 106, Oct. 2011.

[15] A. D. Falco, C. Conti, and G. Assanto, "Quadratic phase matching in slot waveguides," *Opt. Lett.,* vol. 31, no. 21, pp. 3146–3148, Nov. 2006.

[16] C. Koos, L. Jacome, C. Poulton, J. Leuthold, and W. Freude, "Nonlinear silicon-on-insulator waveguides for all-optical signal processing," *Opt. Exp.,* vol. 15, no. 10, pp. 5976–5990, May 2007.

[17] R. Spano *et al.,* "Group velocity dispersion in horizontal slot waveguides filled by Si nanocrystals," in *Proc. IEEE Int. Conf. Group IV Photon.,* 2008, pp. 314–316.

[18] P. B. Johnson and R. W. Christy, "Optical constants of the noble metals," *Phys. Rev. B, Condens. Matter,* vol. 6, no. 12, pp. 4370–4379, Dec. 1972.

[19] K. Tarnowski, B. Kibler, C. Finot, and W. Urbanczyk, "Quasi-phase-matched third harmonic generation in optical fibers using refractive-index gratings," *IEEE J. Quantum Electron.,* vol. 47, no. 5, pp. 622–629, May 2011.

[20] S. Hernandez *et al.,* "Linear and nonlinear optical properties of Si nanocrystals inSiO$_2$ deposited by plasma-enhanced chemical-vapor deposition," *J. Appl. Phys.*, vol. 103, no. 6, pp. 064309-1–064309-6, Mar. 2008.

[21] V. Grubsky and A. Savchenko, "Glass micro-fibers for efficient third harmonic generation," *Opt. Exp.*, vol. 13, no. 18, pp. 6798–6806, Sep. 2005.

[22] G. V. Prakash, M. Cazzanelli, Z. Gaburro, and L. Pavesi, "Nonlinear optical properties of silicon nanocrystals grown by plasma-enhanced chemical vapor deposition," *J. App. Phys.*, vol. 91, no. 7, pp. 4607–4610, Apr. 2002.